Appl Phys A (2014) 115:263–273
DOI 10.1007/s00339-013-7804-2

Applied Physics A
Materials Science & Processing

Fabrication and spectral investigation of Y_2O_3:Nd^{3+} nanoparticles

G. Bilir · G. Ozen · J. Collins · B. Di Bartolo

Received: 19 February 2013 / Accepted: 30 May 2013 / Published online: 26 June 2013

Abstract In this study we have synthesized Y_2O_3 (yttria) nanopowders with 1 % Nd^{3+} concentration by using a thermal decomposition method and investigated the effect of annealing temperature on the particle sizes and the effect of particle sizes on the spectroscopic properties of these systems. The particle sizes were effectively controlled by synthesis and annealing temperatures; the sizes were found to vary in the 15–290 nm range. The particle sizes and cubic phase of the yttria were determined by using XRD patterns and confirmed by SEM and TEM measurements. We note that the particle sizes increase by increasing the synthesis and annealing temperatures. Temperature dependence of the width and position of a selected spectral line were successfully fitted with the theoretical expressions. We studied thoroughly the behavior of the samples under pulsed excitation and give plausible explanations of the measured effects.

1 Introduction

New avenues to research have been opened by the fabrication of nanopowders doped with optically active ions. Experimental results indicate that the energy levels are not much affected by the spatial confinement, whereas the dynamical properties are dependent on the size of the nanoparticles. Another important result indicates that nanopowders doped with optically active ions may luminesce even when the dopant concentration exceeds the maximum concentration at which solids of the same nature can emit luminescent radiation [1, 2].

The problem of the role played by the particles' surfaces versus their inner parts needs investigation, especially in regard to the setting of the phonon spectrum in the presence of the spatial confinement.

Thermal decomposition is a powerful and cheap wet chemical technique that can be used to synthesize Y_2O_3 nanopowders. This process is based on the chemical decomposition of the materials caused by heat [3]. In this study we used thermal decomposition to synthesize Y_2O_3 nanopowders. The compositions of the prepared formulations, synthesis and annealing temperatures, and mean particle sizes are given in Table 1.

2 Experimental

2.1 Preparation of the Nd^{3+}-doped Y_2O_3 powders

Nanosized Y_2O_3 samples doped with 1.0 % mol Nd^{3+} ion concentration were prepared by thermal decomposition of yttrium–neodymium alginate. Yttrium nitrate hexahydrate $Y(NO_3)_2{\cdot}6H_2O$, neodymium nitrate hydrate $Nd(NO_3)_3{\cdot}H_2O$, and low-viscosity (250 cps of 2 % solution) alginic acid sodium salt of an analytic grade were purchased from the Sigma Aldrich Company.

The yttrium–neodymium alginate beads were prepared by a thermal decomposition method according to the prescription given in the literature [3]. 0.2 M 100 ml yttrium–neodymium nitrate solution was prepared by dissolving the

G. Bilir (✉) · G. Ozen
Department of Physics, Istanbul Technical University, Istanbul, Turkey
e-mail: bilir@bc.edu

J. Collins
Department of Physics, Wheaton College, Norton, MA, USA

G. Bilir · B. Di Bartolo
Department of Physics, Boston College, Chestnut Hill, MA, USA

Table 1 Formulations of yttrium–neodymium alginate solution prepared, synthesis and annealing temperatures, and mean particle sizes obtained from the Scherrer equation

Alginate (% w/w)	Yttrium nitrate (molar)	Neodymium nitrate (molar)	Synthesis temperature (°C)	Annealing temperature (°C)	Mean size (nm)
1	99 % of 0.2M	1 % of 0.2M	350	–	13.8
			400	–	16.0
			450	–	20.4
			500	–	27.1
			500	600	32.3
			500	800	40.0
			500	1000	49.7
			500	1400	248.2

appropriate amounts of the yttrium nitrate and neodymium nitrate salts in ultra-pure water. Also, 50 ml alginate solution with 1 % w/w concentration was prepared by dissolving an appropriate amount of the sodium alginate salt in the ultra-pure water under magnetic stirring.

Alginate is a biopolymer which is extracted from three species of brown algae. It is a linear heteropolysaccharide composed of D-mannuronic acid and L-guluronic acid. Gelation of alginate is possible by the interaction of the carboxylate group with divalent ions and the formation of beads can be achieved by dropwise addition of sodium alginate into divalent solution by using a syringe with a needle or pipette [3, 4]. The formation of the yttrium–neodymium alginate beads was achieved by the dropwise addition of the sodium alginate solution into yttrium–neodymium salt solution by using a syringe.

The prepared beads were kept in their gelling medium for 30 min under gentle stirring; then they were removed from their gelling medium, placed in a porcelain crucible, and heated to different temperatures ranging from 350 to 500 °C for 24 h with a heating rate of 10 °C/min in an electric furnace in air medium. Some of the products obtained were annealed at 600, 800, 1000, and 1400 °C, to investigate the particle size dependence on the annealing temperature.

2.2 Structural characterization

X-ray diffraction (XRD) investigations were carried out with a Bruker AXS D8 model (Cu-Kα radiation) diffractometer at 40 kV and 30 mA setting in the 2θ range from 20 to 70° with a scanning step of 0.02°. A JEOL 6335F model scanning electron microscope (SEM) was used to get SEM images of the samples. Elemental analysis was made by using energy dispersive spectroscopy (EDS) attached to the SEM. TEM images of the samples were obtained by using a JEOL 2010F model transmission electron microscope (TEM) operated at 200 kV with a field emission gun. TEM specimens were prepared by depositing a few drops of a sample, dispersed in ethanol by using an ultrasonic bath, on a carbon-coated copper grid.

2.3 Spectroscopic measurements

The continuous emission spectra of the samples were obtained by pumping the samples with the output of a Laser Drive Inc. model LDI-820 laser diode, that resulted in the excitation of the levels $^2H_{9/2}$–$^4S_{5/2}$. The luminescence signal was directed toward the entrance slit of a 1 m McPherson model 2051 monochromator and chopped at a frequency of 250 Hz before entering the slit. The monochromator provided a resolution 0.8 Å with the slits set at 50 μm and a wavelength reproducibility of 0.1 Å.

The optical signal was detected by a Hamamatsu 7102 photomultiplier tube with an S1 response, sent to a EG&G model 5210 lock-in amplifier, and recorded in a computer.

The same arrangement was used for the line-width and line-shift measurements with the entrance and output slits of the monochromator set at 80–150 μm, which corresponds to a 1–2 Å spectral width and a 5 Å/min scanning rate.

The experimental data on the responses of the samples to pulsed excitation were obtained by using a Schwarz Electro-Optics Inc. model Titan-P titanium–sapphire laser and a Tektronix model TDS3052B oscilloscope.

For the experiments in the temperature range 34–300 K, the samples were mounted on the cold finger of a closed-cycle helium refrigerator. This system uses a Janis Research model RD dewar connected with a Leybold model RW2 compressor. The temperature was controlled by using a Lake Shore Cryotonics 805 model controller. For the experiments at higher temperatures the samples were placed on a hot plate which provided up to 700 K temperatures and the surface temperatures of the samples were precisely measured by using a J-type thermocouple.

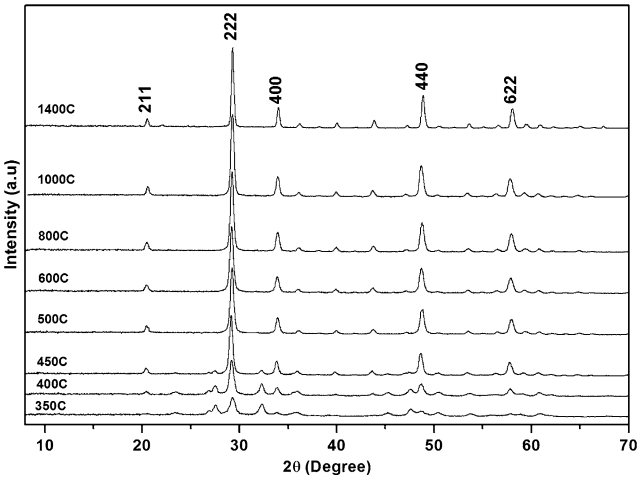

Fig. 1 XRD patterns of the 1 % Nd^{3+} doped Y_2O_3 nanopowders

3 Experimental results

3.1 Structural characterization

The XRD patterns of the 1 % Nd^{3+} doped Y_2O_3 samples are given in Fig. 1. The crystal structure and phase of all samples were analyzed by using these patterns. The cubic phase of the yttria without any other phases was identified by comparing the peak positions and the intensities with those in the Joint Committee on Powder Diffraction Standards (JCPDS) data files. It was clearly seen that the peak positions correspond well to the standard card with number 41-1105.

Figure 2 shows the SEM images of the as-prepared (500 °C) and annealed at 1000 °C Y_2O_3 samples. The nanopowders with spherical shapes are relatively uniform and have average diameters of ∼30 nm and ∼50 nm in as-prepared (500 °C) and annealed (1000 °C) samples, respectively. It is clearly seen from the SEM images that the particle sizes of the samples are strongly dependent on the synthesis and annealing temperatures and show an increasing tendency with increasing annealing temperature. Also, SEM images confirmed the particle sizes estimated from XRD measurements by using the Scherrer equation. The inset of Fig. 2 shows the EDS (energy dispersive X-ray spectroscopy) spectra of the samples.

We also conducted a series of TEM measurements to confirm the particle sizes and the morphologies of the synthesized samples. Representative TEM images are given in Fig. 3. It is clearly seen from the micrographs that the particle sizes are in good agreement with the results obtained from both XRD and SEM measurements.

3.2 Spectroscopic characterization

The measurements of continuous luminescence spectra were conducted from 35 to 300 K and in the 850–1150 nm wavelength range. The luminescence spectra of all the samples at 35 and 300 K and the corresponding energy level scheme are given in Figs. 4a and 4b and Fig. 5, respectively. The emission spectra of the samples consist of two group of emission peaks due to the $^4F_{3/2} \rightarrow {}^4I_{9/2}$ and $^4F_{3/2} \rightarrow {}^4I_{11/2}$ transitions. We note that the general aspect of the spectra is the same for all the samples. The intensity of the emission lines increases for all samples with decreasing temperature; it is also found to increase with increasing particle sizes. The spectra with greatest intensity are those of the crystal. Examining the spectra in detail, we see that the smaller the size of the particles, the wider the spectral lines and the greater the shift of each line toward longer wavelengths with respect to the corresponding line in the crystal. Figure 6 presents the shift of a well-isolated line at 914.5 nm with respect to the corresponding line in the crystal. This is the line we have chosen in order to study the effects of temperature on the width and position of the spectral lines of the samples. The results of these measurements are reported in Figs. 7 and 8.

The measurements of the response of the samples to pulsed excitation were carried out in the 35–700 K temperature range. The results are given in Figs. 9a–9d. Since the luminescence output of the Nd-doped samples consists of spectral lines related to transitions that initiate in the doublet $^4F_{3/2}$, the response of these systems to pulsed excitation is the same, regardless of the spectral line at which it is measured. We have chosen to measure this response at $\lambda = 892.5$ nm (see Fig. 5). The lifetime of the $^4F_{3/2}$ doublet is host-dependent: it is 480 μs in YLF [5], 230 μs in YAG [6, 7], 33 μs in YVO_4 [5, 6], and 260 μs in Y_2O_3 [7], etc., but it is generally independent of temperature due to the large gap between the $^4F_{3/2}$ doublet and the lower $^4I_{15/2}$ multiplet [8]. We have found that the lifetime of the $^4F_{3/2}$ doublet in the Y_2O_3 crystal, the value ∼250 μs, almost independent of temperature.

The response pattern of the crystal is close to an exponential, more so at high temperatures. The response of the powder samples deviates from exponential at early times and then becomes exponential with a decay constant greater than that of the crystal, so that at a time after the initial response the two patterns (the pattern of the crystal and that of the sample) cross over.

The smaller the particle and the lower the temperature, the greater the deviation of the initial pattern from exponentiality and the longer the time at which the two patterns cross. Figure 10 presents the lifetimes of all the samples as a function of temperature. When a decay pattern was exponential, the lifetime was calculated from an exponential fit. When a decay pattern was not exponential, we took as a measure of the lifetime the area under the decaying signal, having set the intensity of the initial signal equal to one.

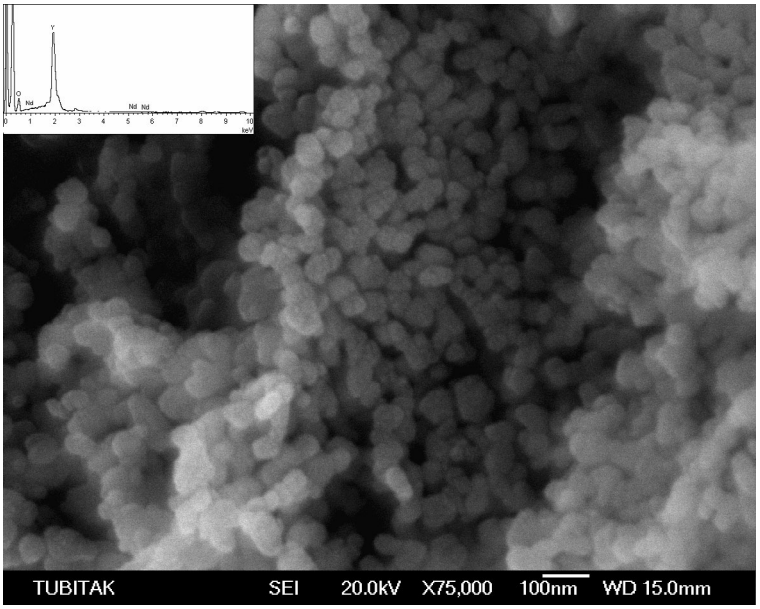

a

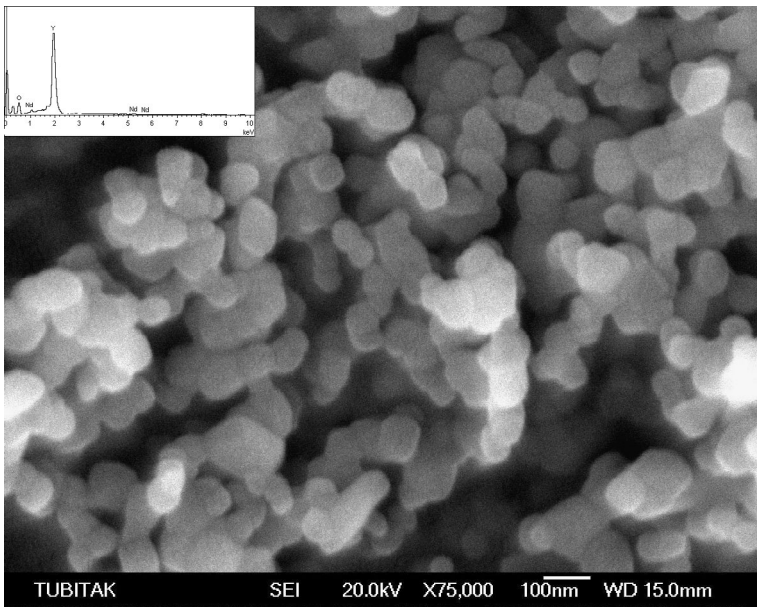

b

Fig. 2 (**a**) SEM image of as-prepared (500 °C) 1 % Nd^{3+} doped Y_2O_3 nanopowders (*inset*: corresponding EDS spectrum); (**b**) SEM image of 1 % Nd^{3+} doped Y_2O_3 nanopowders annealed at 1000 °C (*inset*: corresponding EDS spectrum)

4 Discussion of results

4.1 Structural properties

The cubic phase of the yttria was determined by using XRD patterns. It was observed that the lattice parameter increases with the addition of dopant ions and was found to be up to 10.6051 Å, which is the proof of the incorporation of the Nd ions into Y^{3+} sites due to the larger ionic radius of Nd^{3+} (112.3 pm) than Y^{3+} (104 pm) [9, 10]. It was observed that the widths of the diffraction lines broadened with decreasing temperature because of the decreasing crystalline sizes. The narrowest line was observed for the sample annealed at 1400 °C. The particle sizes of the powders were estimated by using the Scherrer equation [11] reported below:

$$L = \frac{K\lambda}{\beta \cos\theta}, \tag{1}$$

where L is the crystallite length, K is a constant that varies with the method of taking the breadth ($0.89 < K < 1$), λ is the wavelength of the incident X-ray beam, β is the width of

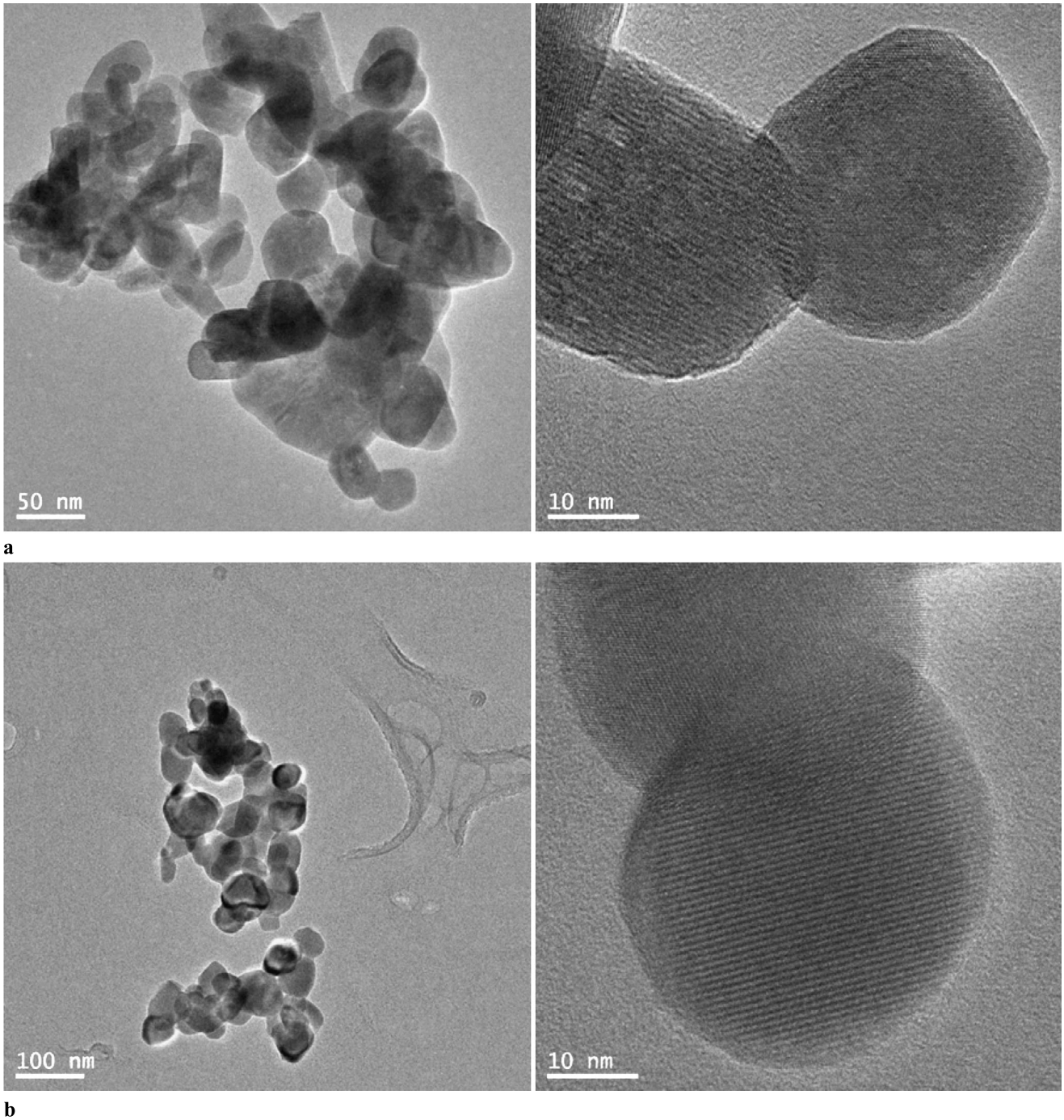

Fig. 3 Representative TEM micrographs of 1 % Nd^{3+} doped Y_2O_3 sample (**a**) synthesized at 350 °C; (**b**) annealed at 1000 °C

the peak at half maximum intensity of a specific phase (hkl) in radians, and θ is the center angle of the peak. The (222) peaks were used to estimate the particle sizes. As seen from Fig. 1 and our calculations given in Table 1, the particle size of the samples increases with increasing annealing temperature. Also, the breadth of the XRD peaks decreases with increasing annealing temperature.

The SEM and TEM images confirmed the particle sizes calculated by using the Scherrer equation. A nebulous structure which we attributed to the existence of an organic compound (alginate) was seen in some samples' SEM images. This structure disappears with increasing annealing temperature. On the other hand, the EDS results confirm the presence of Nd^{3+} content. All of the structural characterization

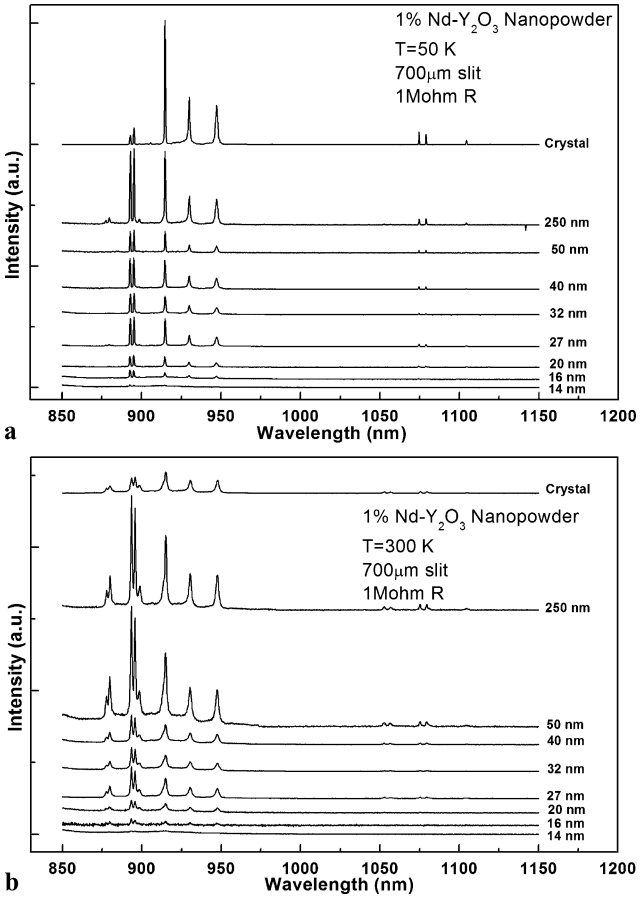

Fig. 4 (**a**) Continuous emission spectra of samples at 50 K. (**b**) Continuous emission spectra of samples at 300 K

measurements showed that the particle sizes can be effectively controlled by the synthesis and annealing temperatures, and increase with increasing treatment temperature.

4.2 Spectroscopic response

The general aspect of the spectral output of the powder samples strongly resembles the spectra of the crystal, confirming the fact that the confinement provided by the restrictions of the particles' sizes does not affect by much the energy levels of the Nd^{3+} ion.

The shifts reported in Fig. 6 indicate that their magnitude becomes greater the smaller is the dimension of the particle. It seems then legitimate to attribute this behavior to the increasingly important role played by the surfaces in smaller particles. The Nd ions at the surface are in a different environment with respect to the ions in the interior of the material. In a crystal the ions at the surface are a negligible minority with respect to the ions in the bulk of the material, but in a particle it is not so. In very small particles, going from the surface toward the center of the particle, there is gradation in the Nd–O bond lengths, approaching the conditions of Nd in a single bulk crystal. It is possible that, even in the interior of the particle, the conditions of the environment in the bulk will never be reached. This may account for the fact that the shift of the lines increases with decreasing of the particles' sizes.

The results concerning the thermal line broadening were handled as follows.

The experimental data were compared with the following equation [12]:

$$\Delta E\left(\mathrm{cm}^{-1}\right) = \Delta E_0 + \Delta E^{\mathrm{R}}, \tag{2}$$

where

$$\Delta E^{\mathrm{R}} = \overline{\alpha}\left(\frac{T}{T_{\mathrm{D}}}\right)^7 \int_0^{T_{\mathrm{D}}/T} \frac{x^6 \mathrm{e}^x}{(\mathrm{e}^x - 1)^2}\,\mathrm{d}x. \tag{3}$$

In Eq. (2), ΔE_0 is the temperature-independent residual width from the two levels due to random crystal strains and spontaneous phonon emission processes and ΔE^{R} is the temperature-dependent contribution to the width due to the Raman scattering of phonons: $\overline{\alpha}$, T_{D}, and ΔE_0 are treated as adjustable parameters to get a best fit (a least square fit) to the experimental line-width data shown in Fig. 7.

The values of the parameters that were used to produce the fitting of the experimental data with the theoretical formulas are listed in Table 2. It is of interest to note that the residual line width at low temperature increases with decreasing particle size.

The effect of temperature on the position of the chosen sharp line is presented in Fig. 8. We determined that the line positions are red shifted with increasing temperature. The experimental data were compared with the following Eq. (4) that expresses the shift as due to the process of emission and absorption of virtual phonons [12]:

$$\delta E\left(\mathrm{cm}^{-1}\right) = \delta E^{\mathrm{R}} = \alpha\left(\frac{T}{T_{\mathrm{D}}}\right)^4 \int_0^{T_{\mathrm{D}}/T} \frac{x^3}{\mathrm{e}^x - 1}\,\mathrm{d}x, \tag{4}$$

where α and T_{D} are treated as adjustable parameters to get a best fit. The line position at $T = 0$ K was estimated by extrapolating the experimental data to zero temperature. The corresponding fitting values of α and T_{D} for each line are listed in Table 2.

The fitting values of the coupling coefficients $\overline{\alpha}$ and α obtained for the line widths and line shifts are typical for rare-earth-ion-doped laser crystals. They are usually less than 100 cm^{-1}. In case of transition-metal ions the coupling coefficients $\overline{\alpha}$ and α are usually about 500 cm^{-1} [13, 14].

The decay patterns of the luminescent Nd^{3+} ions embedded in the nanoparticles are expected to deviate from an exponential decay of the same ions in the crystal for two reasons:

(1) The role played by the surfaces will be increasingly important as the radius of the particle is reduced, producing

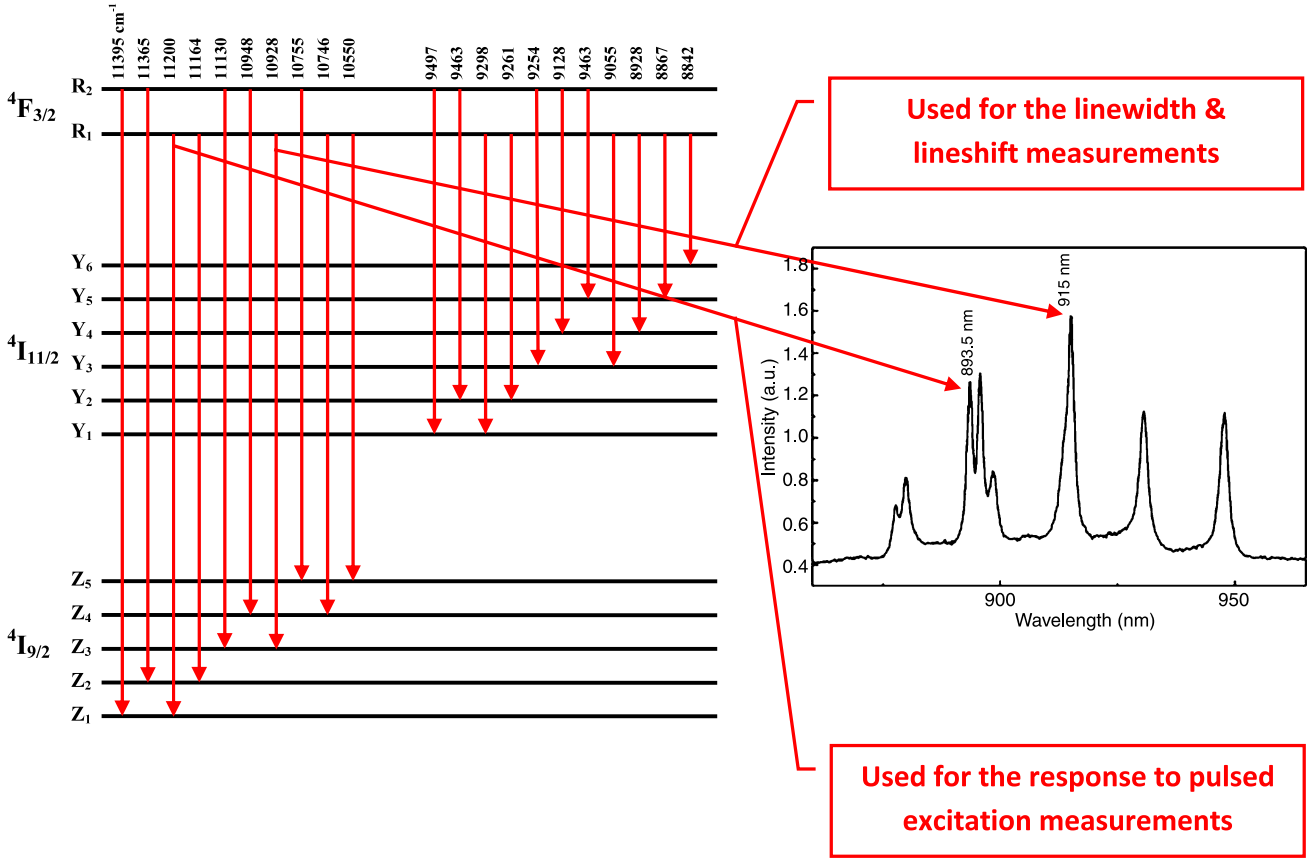

Fig. 5 Energy level scheme of Nd^{3+} in Y_2O_3

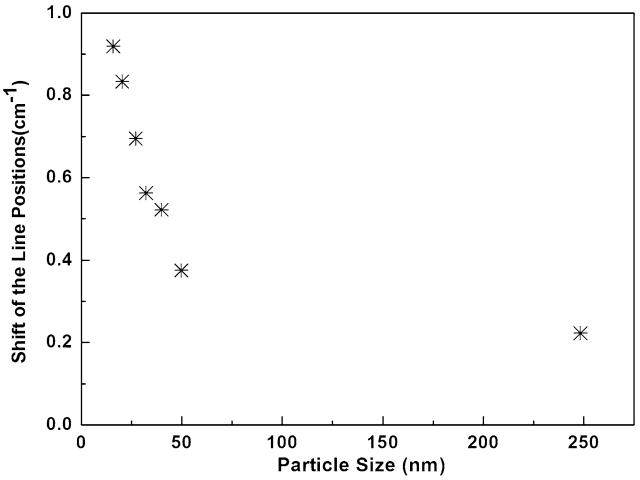

Fig. 6 Red shift of a line position of different samples with respect to the crystal line

a deviation from exponentiality. Molecular groups such as O–H residing on the surface may enhance the decay process due to their stiff vibrations that rob the ion of its excitation energy. We reasonably expect a deviation from exponentiality at the beginning of the decay pattern.

(2) The ensemble of particles in the sample also differs from the bulk material because of the presence of the interstices between the particles. In what follows, we shall describe how we can handle the problem presented by this difference.

The rate of spontaneous relaxation of an atomic system is given by [15]

$$A(\Psi J, \Psi' J') = \frac{64\pi^2(\Delta E)^3}{3h(2J+1)}\eta F^2, \tag{5}$$

where F is the matrix element of the electric dipole operator, ΔE is the energy gap between the states $|\Psi J\rangle$ and $|\Psi' J'\rangle$, and $\eta = \frac{n(n^2+2)^2}{9}$; Lorentz correction is applied for the local field with $n =$ index of refraction of the host material.

Applying those considerations to the ions embedded in the nanoparticles, we can say that the rate of their spontaneous emission (inverse of the radiative lifetime) depends on an effective index of refraction n_{eff}, which consists of a combination of the index of refraction of the nanoparticle n_{NP} and of the index of refraction of the surrounding medium n_{med}:

$$n_{\text{eff}}(x) = \chi n_{\text{NP}} + (1-\chi) n_{\text{med}}, \tag{6}$$

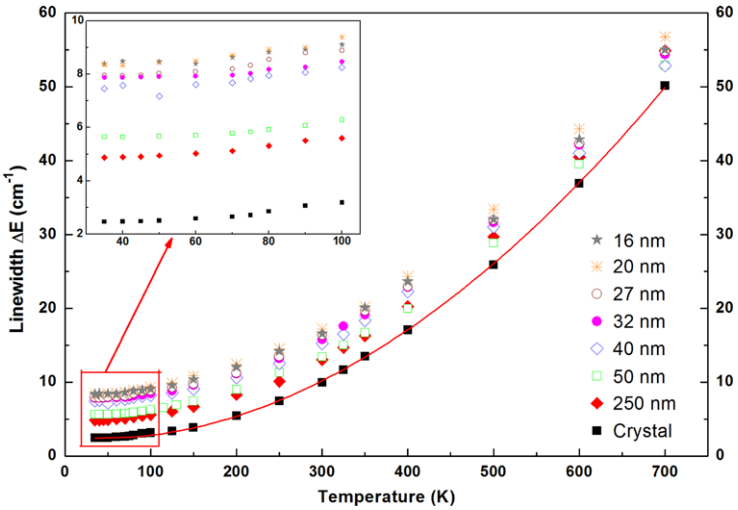

Fig. 7 Variation of line width as a function of temperature in 1 % Nd^{3+} doped Y_2O_3. The *dots* are experimental results and the *solid curve* is the theoretical fitting with respect to the crystal line

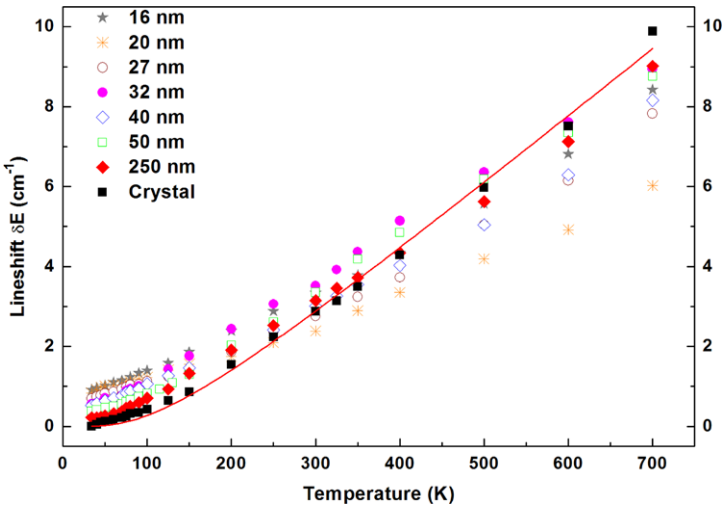

Fig. 8 Line shift as a function of temperature in 1 % Nd^{3+} doped Y_2O_3. The *solid red line* is the theoretical fitting to the crystals' experimental data

where χ is the filling factor indicating the fraction of space that is occupied by the nanoparticles. The validity of the usage of n_{eff} in calculating the probability of decay rests on the fact that the size of the particles is much smaller than the wavelength of light [16].

Since the ratio χ is independent of the size of the nanoparticles, the tails of the response patterns of the particles with different sizes should be parallel after they cross the pattern corresponding to the crystal response to pulsed excitation.

The responses of the samples to pulsed excitation present the following interesting aspects:

(1) At each temperature the decay patterns depend on the size of the particles with increasingly greater deviation from exponentiality for smaller particles (see Figs. 9a–9d).
(2) The patterns that deviate from exponentiality eventually cross the exponential pattern of the crystal. The greater the deviation, the more distant in time is the crossing. A possible explanation of these experimental findings is the existence of a large amount of O–H groups at the surface of each particle, which, considering the stiff O–H vibration, could provide a quenching of the luminescence and a shortening of the lifetime.
(3) All the decay patterns of the particles of different sizes become parallel after they cross the decay pattern of the ions in the crystal. This behavior indicates that the effective index of refraction is lower for the nanoparticles than for the single crystal, hence decreasing the radiative decay rate, and the filling factor χ is independent of the particles' size.

5 Conclusions

This study was focused on the synthesis and characterization of Y_2O_3 nanophosphors doped with 1 % neodymium (Nd^{3+}) ions. Nanoparticles were synthesized by using the

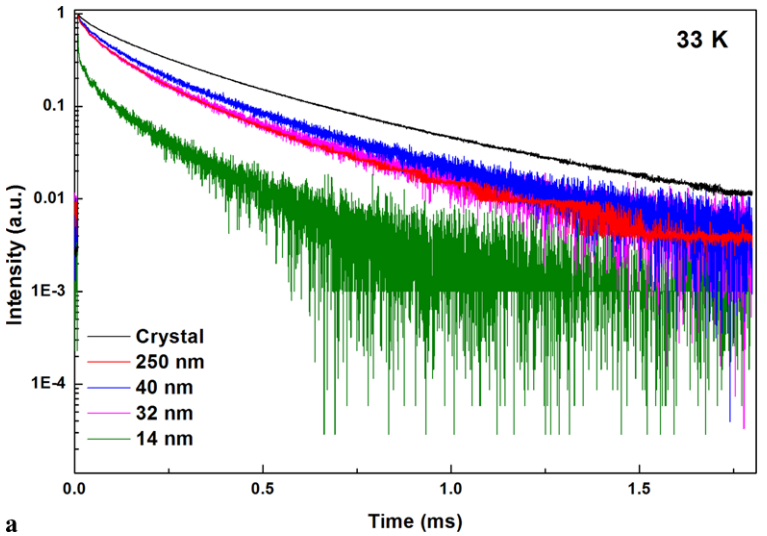

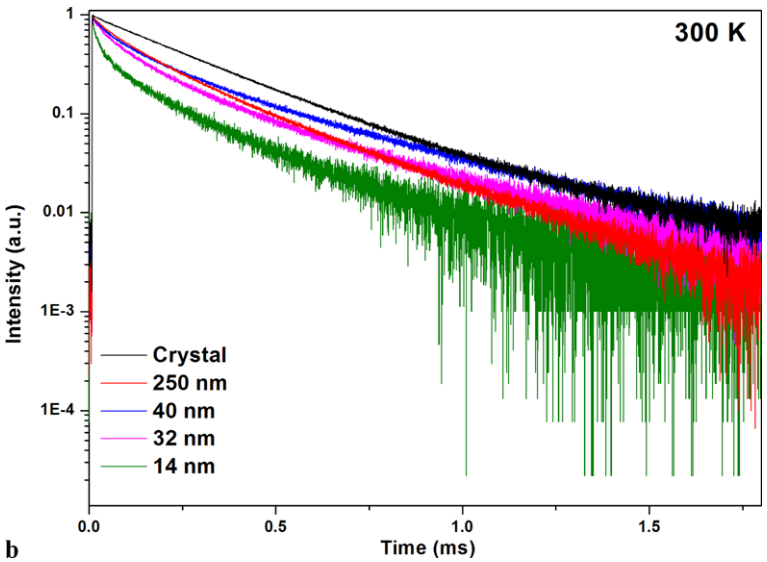

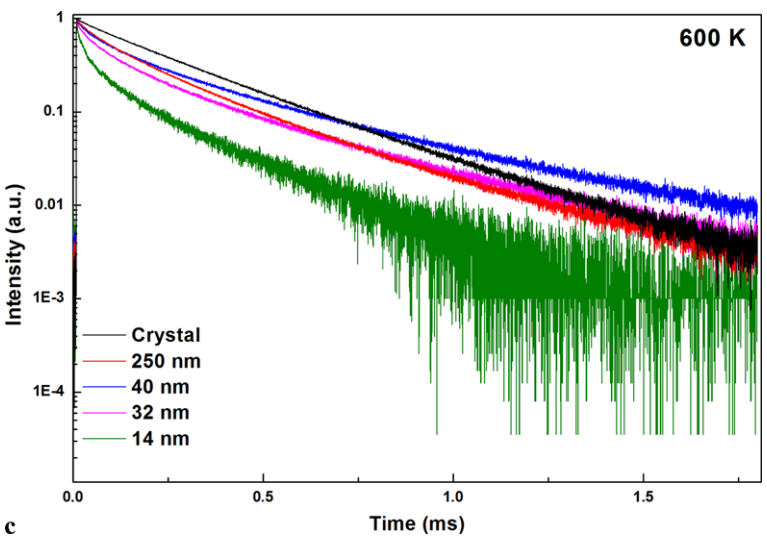

Fig. 9 Response to pulsed excitation results of all powders at (**a**) 33 K, (**b**) 300 K, (**c**) 600 K, (**d**) 700 K

Fig. 9 (*Continued*)

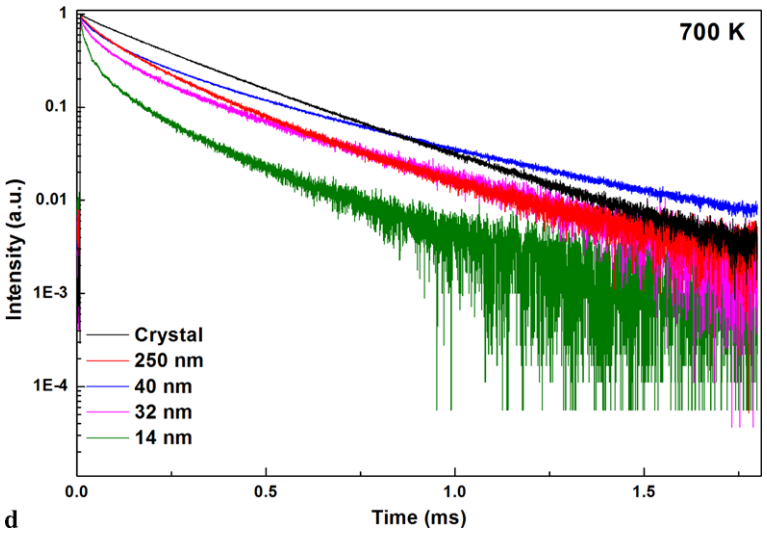

Fig. 10 Variation of lifetimes with the temperature

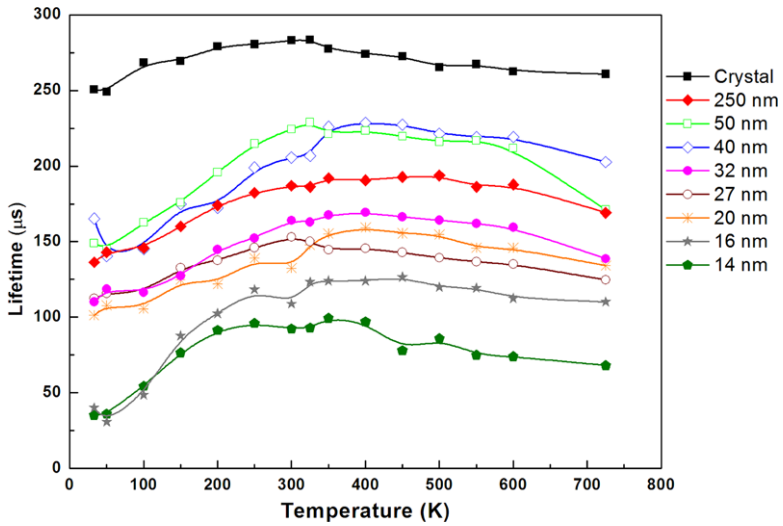

thermal decomposition technique and annealed at different temperatures to control particle sizes. The synthesized particles were structurally characterized by using X-ray diffraction (XRD), scanning electron microscopy (SEM), and transmission electron microscopy (TEM). The cubic phase of the Y_2O_3 was determined and the size of the particles was found to range from ∼15 to 300 nm.

A series of spectroscopic measurements on a number of these nanoparticle samples were performed. For comparison we also characterized spectroscopically aY_2O_3 crystal sample.

For each sample the emission spectrum was accurately measured in a wide range of temperatures ranging from 30 to 300 K. The spectra consisted of the Nd^{3+} ion's narrow spectral lines corresponding to transitions from the $^4F_{3/2}$ doublet level to the $^4I_{11/2}$ and $^4I_{9/2}$ manifolds.

We also measured the width and the position of a well-isolated line in the temperature range 30–700 K. The results indicate that the residual width at low temperatures is larger for powders with smaller particle sizes.

Table 2 Best fit parameters (α, $\overline{\alpha}$, T_D, and ΔE_0) obtained from line-shift and line-width measurements

Particle size	Line shifts		Line widths		
	T_D [K]	α [cm^{-1}]	ΔE_0 [cm^{-1}]	T_D [K]	$\overline{\alpha}$ [cm^{-1}]
Crystal	429	22	2.46	440	95
248.2 nm	285	12	4.88	397	80
49.7 nm	263	11	5.65	360	62
40 nm	258	9.1	7.46	305.7	44
32.3 nm	207	8.3	7.88	305.5	46
27.1 nm	352	12	7.96	210	21
20.4 nm	236	5.7	8.36	109	5.9
16 nm	272	9.5	8.40	194	18

Finally, measurements were performed on the decay patterns of Nd^{3+} ions following a pulsed excitation. These measurements were conducted in the temperature range 30–700 K. Such patterns vary considerably with the size of the nanoparticles, so that they may be considered signatures of these sizes. When comparing the decay patterns of the powders with the exponential decays of the Y_2O_3:Nd^{3+} crystal, we found larger deviations from exponentiality for the powders of smaller particle sizes, and smaller deviations from exponentiality at high temperatures.

Acknowledgements One of the authors (G. Bilir) would like to thank the Scientific and Technological Research Council of Turkey (TUBİTAK) for its support. All the authors would like to thank Dr. Dezhi Wang of Boston College for his support with the XRD and TEM measurements and Dr. Maura Cesaria of the University of Lecce for her valuable suggestions.

References

1. R.E. Muenchausen, L.G. Jacobsohn, B.L. Bennett, E.A. McKigney, J.F. Smith, J.A. Valdez, D.W. Cooke, J. Lumin. **126**, 838 (2007)
2. X. Qin, Y. Ju, S. Bernhard, N. Yao, J. Mater. Res. **20**, 2960 (2005)
3. S. Baskoutas, P. GiaBouranis, S.N. Yannopoulos, V. Dracopoulos, L. Toth, A. Chrissanthopoulos, N. Bouropoulos, Thin Solid Films **515**, 8461 (2007)
4. W.R. Gomboltz, S.F. Wee, Adv. Drug Deliv. Rev. **31**, 267 (1998)
5. W. Koechner, *Solid State Laser Engineering*, 6th edn. (Springer, Berlin, 2006), p. 57
6. R. Moncorgé, in *Spectroscopic Properties of Rare Earths in Optical Materials*, ed. by G. Liu, B. Jacquier (Springer, Berlin, 2005), p. 333
7. C. Fouassier, in *Encyclopedia of Inorganic Chemistry*, 2nd edn., ed. by R.B. King (Wiley, New York, 2005)
8. S. Singh, W.A. Bonner, W.H. Grodkiewicz, M. Grasso, L.G. Van Uitert, Appl. Phys. Lett. **29**, 343 (1976)
9. Y.Q. Jia, J. Solid State Chem. **95**, 184 (1991)
10. R. Srinivasan, N.R. Yogamalar, J. Elanchezhiyan, R.J. Joseyphus, A.C. Bose, J. Alloys Compd. **496**, 472 (2010)
11. P. Scherrer, Gött. Nachr. Ges. **2**, 98 (1918)
12. B. Di Bartolo, *Optical Interactions in Solids*, 2nd edn. (World Scientific, Singapore, 2010), p. 385
13. J.T. Karpick, Nuovo Cimento B **7**, 62 (1972)
14. X. Chen, B. Di Bartolo, N. Barnes, B. Walsh, Phys. Status Solidi B **241**, 1957 (2004)
15. M.F. Reid, in *Crystal Field Handbook*, ed. by D.J. Newman, B. Ng (Cambridge University Press, Cambridge, 2000), p. 190
16. G. Liu, X. Chen, in *Handbook on the Physics and Chemistry of Rare Earths*, vol. 37, ed. by K.A. Gschneidner, Jr., J.-C.G. Bünzli, V.K. Pecharsky (Elsevier/North-Holland, Amsterdam, 2007), p. 90. Chap. 233